New Astronomy 60 (2018) 88–94

Contents lists available at ScienceDirect

New Astronomy

journal homepage: www.elsevier.com/locate/newast

A pilot investigation to constrain the presence of ring systems around transiting exoplanets

W. Timothy Hatchett*, Jason W. Barnes, John P. Ahlers, Shannon M. MacKenzie, Matthew M. Hedman

Department of Physics, University of Idaho Moscow, Idaho 83844-0903, USA

ARTICLE INFO

Keywords:
Techniques:photometric
Eclipses
Planetary systems
Rings

ABSTRACT

We demonstrate a process by which to evaluate the presence of large, Saturn-like ring systems around transiting extrasolar giant planets. We use extrasolar planet candidate KOI-422.01 as an example around which to establish limits on the presence of ring systems. We find that the spherical-planet (no-rings) fit matches the lightcurve of KOI-422.01 better than a lightcurve with a planet having obliquity angles 90°, 60°, 45°, or 20°. Hence we find no evidence for rings around KOI-422.01, but the methods that we have developed can be used for more comprehensive ring searches in the future. If the Hedman (2015) low-temperature rings hypothesis is correct, then the first positive detection of exorings might require transits of very long period ($\gtrsim$10 yr) giant planets outside their stars' ice lines.

1. Introduction

Rings surround all of the giant planets in our Solar System, and so it is reasonable to expect that at least some of the planets around distant stars might also have rings. Furthermore, the known rings exhibit a wide range of properties, and it is still not clear why the different planets possess such different ring systems. Jupiter, for example, is the largest planet in our Solar System and has the most massive satellite system, but strangely its rings are the most tenuous of all the giant planets, probably consisting primarily of debris knocked off of its various small moons (Burns et al., 2004). Similarly, both the ice giants Neptune and Uranus have ring systems dominated by narrow ringlets that consist of very dark material, but Neptune's rings are far more tenuous than Uranus'. Why does Uranus have several complete rings with sufficient optical depth to be detectable in occultations (French et al., 1991), while the only parts of Neptune's rings that are detectable in this way are a few arcs in one ring (Cruikshank and Matthews, 1995)?

Saturn, of course, has the most extensive ring system. Indeed, Saturn's rings are so large and bright that they could be seen by the earliest telescopes (Galilei, 1989). However, even after 400 years of study no one can say for certain why Saturn has such an exceptional set of rings. Observations of rings around 'exoplanets', or 'exorings', could therefore help us to better understand what sorts of rings a planet is likely to have.

Additional examples of ringed planets would also help answer the still-contentious question of how dense, extensive ring systems are formed. While various scenarios have been proposed for Saturn's rings (Charnoz et al., 2009a) including disruption of a passing centaur (Charnoz et al., 2009b), tidal breakup of a Kuiper Belt Object (Hyodo et al., 2016), or a moon that migrated too close to the planet (Canup, 2010), each of these scenarios have potentially significant issues. For example, if Saturn's rings formed early from something like a migrating moon, it is not obvious how the rings would remain so bright after being polluted by 4.5 billion years' worth of dark cometary debris (Cuzzi and Estrada, 1998). On the other hand, if the rings formed more recently from the disruption of a large comet or centaur, then it is surprising that similar rings do not exist around the other giant planets, which are much more likely to capture such objects (Charnoz et al., 2009b).

The recent discovery of rings around the centaur 10,199 Chariklo (Braga-Ribas et al., 2014) and possibly 2060 Chiron (Ortiz et al., 2015; Ruprecht et al., 2015; Thiessenhusen et al., 2002) reveals that rings can be found around small bodies and thus has forced scientists to reconsider the question of how rings form. On the one hand, this finding suggests that rings could be found under a wider variety of conditions than previously considered. On the other hand, it is not clear why these objects possess dense rings while objects like Ceres and Pluto, for instance, do not, and so the conditions for ring formation remain obscured.

Thus far, no-one has found evidence for dense rings around any planets outside our Solar System. While a 'ring-like' system was recently

* Corresponding author.
E-mail address: hatc4410@vandals.uidaho.edu (W.T. Hatchett).

https://doi.org/10.1016/j.newast.2017.11.001
Received 28 April 2016; Received in revised form 3 April 2017; Accepted 2 November 2017
Available online 04 November 2017
1384-1076/

found around the companion to the star 1SWASP J140747.93–394542.6 (Mamajek et al., 2012), this 'J1407b' system is very large, with a radius on the order of 0.6 AU (Kenworthy and Mamajek, 2015). Since 0.6 AU is much larger than the Roche limit for J1407b, this ring-like system might be better described as a proto-satellite disk than as a conventional planetary ring. The rings of Saturn and Uranus lie close enough to their host planets for tidal forces to prevent material from aggregating into isolated objects like moons, but the J1407b disk extends far enough that its constituent particles should coalesce into moons in astronomically short timescales. Still, this discovery bodes well for current efforts to find Saturn-like rings around extra-solar planets.

Several different methods have been proposed to detect exorings, including detailed modeling of transit lightcurves (Barnes and Fortney, 2004), phase functions (Arnold and Schneider, 2004; Dyudina et al., 2005), and Rossiter–McLaughlin-like radial velocity data (Ohta et al., 2009). Recently, Santos et al. (2015) determined that the anomalously strong reflected light signature from 51 Peg b (Martins et al., 2015) does not represent a ring system.

In this paper we describe a pilot investigation of a handful of *Kepler* giant planets to explore the feasibility of constraining the presence of exorings with the transit lightcurve technique. In Section 2 we explain our process for choosing which candidates to investigate. Section 3 describes the *Kepler* data and their reduction. How we model and analyze these systems to determine the presence of rings is explained in Section 4. Section 5 discusses the results from lightcurve fitting, particularly its application to KOI-422. Finally, Section 6 discusses some conclusions and possible implications of finding exorings.

2. Methods

Based on Barnes and Fortney (2004), we explore the constraints on the nature of potential rings around exoplanets that detailed analysis of transit lightcurve s might provide. To do so we use the transit fitting algorithm `transitfitter` (Barnes and Fortney, 2004), which produces synthetic light curves by integrating the total stellar flux blocked by the planet and ring at each timestep.[1] The algorithm uses a Leavenberg–Marquardt system to arrive at best-fit quantities for fitted parameters.

We assume that planetary ring systems have zero thickness and lie in their parent planet's Laplace plane. As shown in Burns et al. (1979), close to a planet (as is the case within the Roche limit for particle breakup) the Laplace plane is essentially identical to the equatorial plane, thus placing rings around the equator of the exoplanet.

2.1. Model parameters

While Barnes and Fortney (2004) forward-calculated theoretical transit lightcurve s of ringed planets, it did not allow for a lightcurve fit using the ringed planet model. Here we update `transitfitter` to explicitly allow for fitting of ringed planet parameters in addition to the standard parameters.

The biggest challenge to fitting using ringed planets comes from geometry. Generalized orientations of rings and their lack of spherical symmetry require that the model fully account for the rings' opening angle and projected orientation. Our fitting algorithm allows the adjustment of the five following ring parameters, also shown in Fig. 1:

1. Inner ring radius (R_i)
2. Outer ring radius (R_o)
3. Normal optical depth (τ)
4. Obliquity (ϕ)

[1] Please email JWB at `jwbarnes@uidaho.edu` for a copy of the source code for the `transitfitter` program.

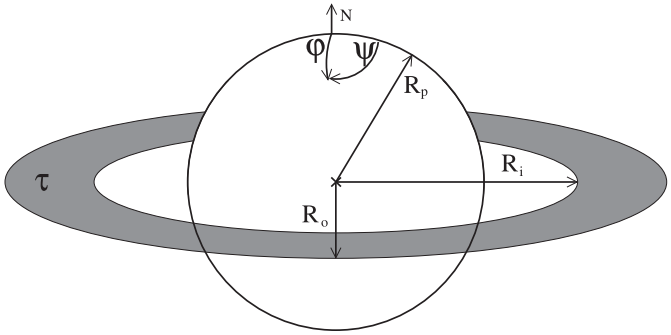

Fig. 1. Fit parameters: obliquity (ϕ), azimuth (ψ), outer radius of rings (R_o), inner radius of rings (R_i), and radius of the planet (R_p).

5. Azimuth angle (ψ)

Assuming a single, uniform ring, the inner radius (R_i) is the distance from the center of the planet to the inner edge of the ring. The outer radius (R_o), likewise, is the distance from the center of the planet to the outer edge of the ring. The area between these two radii within the planet's equatorial plane represents the extent of the rings as determined by the fit.

The normal optical depth τ controls the attenuation ($e^{-\tau}$) through the rings when they are viewed face-on. Solar System rings show a broad range of normal optical depth values, τ, with tenuous systems like Jupiter's main rings and the various tenuous components of the other planet's ring systems having $\tau < 10^{-3}$ (Tyler et al., 1981; Horányi et al., 2009), while some portions of Saturn's B rings have $\tau > 5$ (Colwell et al., 2009). The effective slant optical depth of the rings as viewed in transit will always be equal to or higher than the normal optical depth as a function of the rings' opening angle α.

The opening angle α measures whether the rings present to us edge on ($\alpha = 0°$), face-on ($\alpha = 90°$), or in-between ($0° < \alpha < 90°$). The actual, observed optical depth $\tau_{\rm slant}$ of a planar ring system then becomes $\tau_{\rm slant} = \frac{\tau}{\sin\alpha}$. Note that at $\alpha = 0°$ the observed optical depth is infinite, however its projected area is zero thus this mathematically problematic condition never affects any real fit.

While the opening angle α of the rings is the more direct observable, we instead fit for the more physically relevant planetary obliquity ϕ, the angle between the planet's rotational angular momentum vector and its orbital angular momentum vector (which lies close to orthogonal to the earth's line of sight to the star since the planet transits). Hence when the north pole is pointed towards Earth, the rings are face-on with $\alpha = 90°$ and $\phi \sim \pm 90°$. In this face-on case the lightcurve will be symmetric about the mid-transit point, as shown in Fig. 2.

The rings' observed outline depends not just on how much the planet is tilted, but also on whether it is tilted straight toward you, within the plane of the sky, or somewhere in between. The azimuth angle, ψ, represents the orientation of the planet's rotational angular momentum vector in space, measured clockwise from the plane of the sky as viewed from over the stellar north pole. The ring opening angle α relates to the obliquity ϕ and the azimuth ψ as

$$\alpha = |\sin^{-1}(\sin\phi\ \sin\psi)|. \quad (1)$$

A rotation in ψ will therefore have no effect on the lightcurve if $\phi = 0°$ (edge-on) because the position of the north pole is unaffected; however, the ingress and egress of the lightcurve will typically change as a function of ψ at any other obliquity. Note that, even with a nonzero planetary obliquity ϕ, if the azimuth is $\psi = 0°$ or $\psi = 180°$, then the rings will still appear edge-on.

2.2. Algorithm improvement

The problem of calculating theoretical lightcurves for transiting

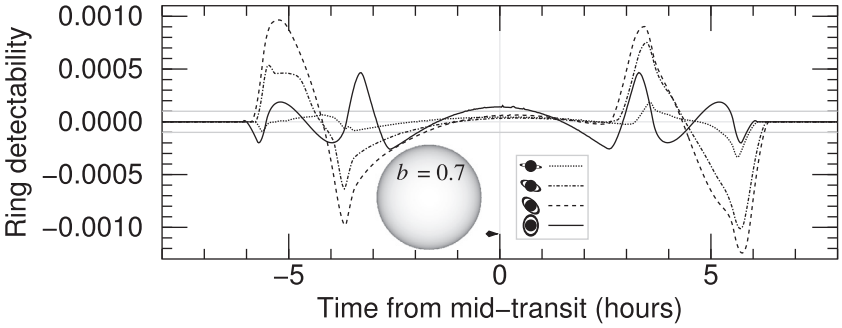

Fig. 2. Theoretical ring detectability of a spherical body by residual, modified from Barnes and Fortney (2004). In this hypothetical case the azimuth angle and impact parameter set to $\pi/4$ and 0.7 respectively. Planetary obliquities of 10° (dotted line), 30° (dashed-dotted line), 45° (dashed line), and 90° (solid line; greatest opening angle) are shown.

ringed planets somewhat resembles that of calculating occultation lightcurves for nearby ringed planets (e.g., French and Nicholson, 2003). The difference is one of distance scales: in the ringed planet case we are far away from the planet and star, which are very close to one another, while in the occultation case we and the planet are very close to one another, and the star is far away (Barnes and Fortney, 2004). Interestingly the calculations by Kenworthy and Mamajek (2015) for the giant disk system J1407b more closely resemble the occultation case due to the large apparent angular width of the rings relative to that of the star as seen from Earth. Because the rings dwarf the star in the J1407b case and the star dwarfs the rings in our case, our theoretical lightcurvegenerating forward model differs in approach from that of Kenworthy and Mamajek (2015).

In its most basic mode, `transitfitter` runs an explicit numerical integral of the stellar flux blocked by a transiting planet in polar coordinates around the projected stellar disk (see Barnes and Fortney, 2003, Equations 9–11). The angular integral in particular performs poorly in the ringed-planet case because it spends most of its time on uncovered areas of the star and the discrete jump onto the covered areas. To improve the computational effort required to fit for ringed planets, we implement a speedup scheme based around integrating only within the covered areas.

We break the angular integral into separate segments, each of which covers a (nearly) uniform blocked flux. First we identify segments for which the planet covers the star. With only the planet blocking starlight across the entire angular integral at this projected radius, we classify this as a Case A(see Fig. 3, upper left), which reverts to the same result as in the no-rings case.

We call the situations where the integration annulus intersects the ring outer edge, but not the inner edge, Case B. Two types of Case B can occur: with one ring segment (Case B1; Fig. 3, upper middle), and with two ring segments (Case B2; Fig. 3, upper right).

When the integration annulus intersects both the inner and outer ring edges, then things get more complex. We call these Case C's. If we end up with two segments in a Case C, then we call it Case C2 (Fig. 3, lower left). Three segments can result if the annulus crosses the ring outer edge four times, but the inner edge only twice: a Case C3 as shown in Fig. 3, lower middle. Four full segments nets a Case C4(Fig. 3, lower right).

In situations where the center of the star's disk, the origin of the coordinate system, is within the ring's inner edge, then the cases reverse. Now Case B results when the annulus crosses the ring's inner edge but not the outer edge, and Case Ctwo results when both edges are crossed. When the origin is *between* the ring edges, or in other words when the rings cover the center of the star, we revert to the explicit numerical integral. All of the cases described in this paragraph only exist near mid-transit and for low transit impact parameters, and thus affect only a small minority of actually computed cases.

After identifying each individual segment, we look for overlaps between planet segments and ring segments. Where planet and ring segments coincide for a given integration annulus, we truncate the ring segment to eliminate the overlap – since the planet blocks all light, there's no need to also add in the ring. Finally, to compute the total flux blocked at this annulus we sum that blocked by the individual segments.

While this approach still requires significant computation to identify edges and to differentiate between the cases, it speeds the process overall by greatly reducing the number of evaluations of opacity that result from the more straightforward explicit numerical integration approach.

2.3. Ring model evaluation

When fitting for ring systems, we hold τ, ψ, ϕ, R_p, and R_i constant on each individual fit and then explore parameter space by running multiple fits over the other parameters.

Holding τ constant enables the fit to converge quickly; without it, the degeneracy between τ and the outer ring radius R_o, which both affect the total transit depth, drives these parameters to unphysical values. Saturn's A and B rings have optical depths ranging from 0.5 and 5 (Colwell et al., 2009). Therefore, our search for exorings varies τ from 0.2 to 5. Below $\tau = 0.2$ the rings start to have little effect on a lightcurve, and above $\tau = 5$ they are sufficiently opaque as to lead to little effect from going higher.

When investigating asymmetric transits, we fix the ring azimuth ψ to values between $0^\circ < \psi < 90^\circ$. Due to the geometrical symmetry of the problem, the transit of two ringed-planet systems, one with azimuth $\psi = x$ and the other with $\psi = -x$, are identical. Similarly, the transit lightcurve s for ringed planets with $\psi = x$ and $\psi = 180^\circ - x$ are the time-inverse of one another.

In the special case where we fit explicitly for symmetric transits, we fix the azimuth $\psi = 90^\circ$ and then adjust the obliquity ϕ to explore the consequences. In doing so, we fit obliquities of $\phi = 90^\circ$,$\phi = 60^\circ$,$\phi = 45^\circ$, and $\phi = 20^\circ$ to span the parameter space. Our spherical-planet fits effectively play the role of $\phi = 0^\circ$, where the rings would be edge-on and undetectable.

Fortney et al. (2007) showed that the radius of a planet is related to the mass and distance from the star. We note from their work that all planet radii are $\lesssim 1.3 R_{Jup}$, but cold gas giants are $\lesssim 1.0 R_{Jup}$, allowing us to hold $R_p = 1 R_{Jup}$ when the spherical model indicates a radius larger than $\sim 1 R_{Jup}$. Although the planet radius could be less than 1 R_{Jup}, we choose this value to reduce the otherwise unwieldy and degenerate parameter space.

We also set $R_i = 1.1 R_{Jup}$ because this produces a gap between the planet and the ring that is comparable in size to the one found interior to Saturn's relatively opaque C ring. Such a gap is expected to occur in any ring system because atmospheric drag will remove material that orbits too close to the planet, and processes like ballistic transport can sharpen the inner edges of dense A and B rings (Estrada et al., 2015). However, while a 0.1 R_{Jup} gap is a reasonable guess for this preliminary study, this parameter should depend on the detailed structure of both the planet's atmosphere and its rings, and so future work will likely need to consider a range of R_i values.

With τ, ψ, ϕ, R_p, and R_i held constant for each individual fit, we

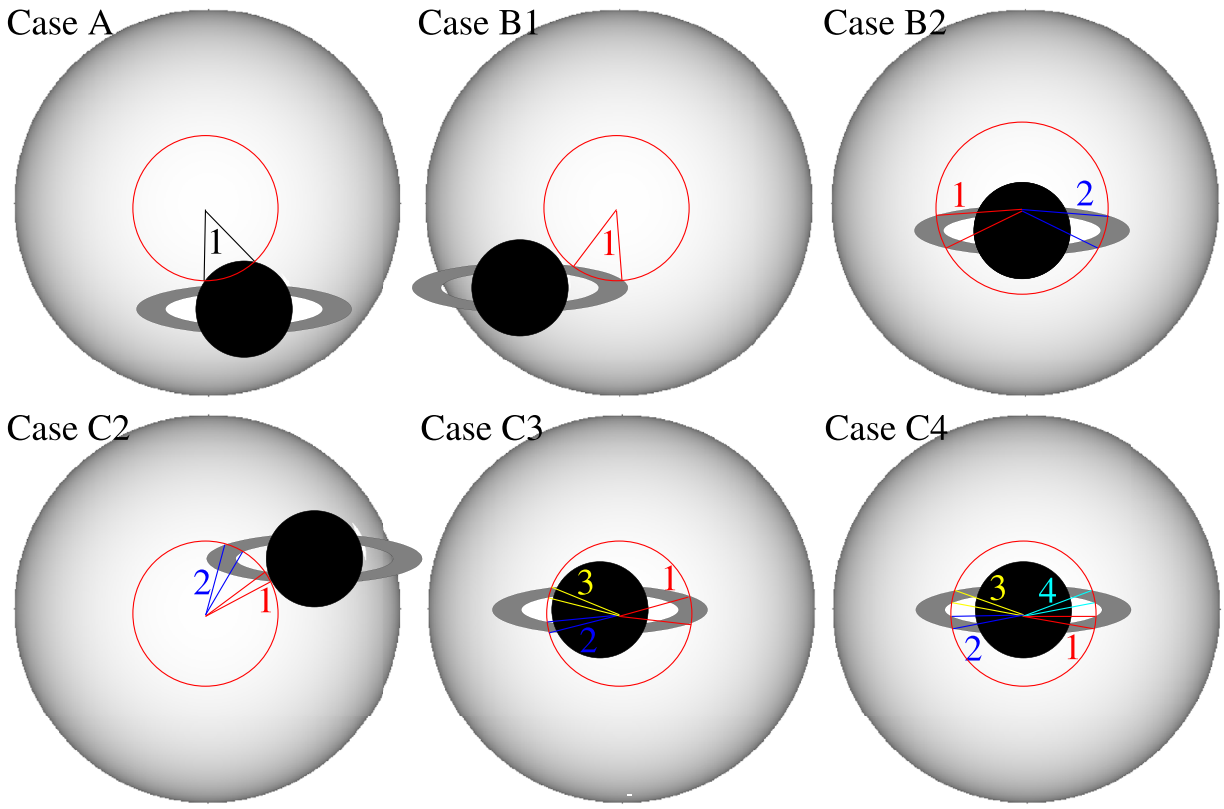

Fig. 3. Here we diagram the six independent cases that our algorithm uses to speed calculations. The limb-darkened white disk represents the star, and the dark outline the planet. The red circle represents one of the numerical annuli around which `transitfitter` integrates in polar coordinates. Case A occurs when the integration annulus in question does not intersect the rings at all. Case B occurs when the annulus intersects the outer edge of the rings, but not the inner edge. And Case C occurs when the annulus crosses both the inner and outer edge of the ring. The number after the Case type indicates how many different azimuthal integration segments are required for that particular sub-case. (For interpretation of the references to colour in this figure legend, the reader is referred to the web version of this article.)

dynamically fit the outer ring radius, star radius, eccentricity, and impact parameter. The spherical model values are used as initial guesses in the ring model. The ring size and orientation are constrained by plotting reduced χ^2 as a function of τ for the various ring angles and normal optical depth.

3. Application

3.1. Candidate considerations

With the goal of finding a single Kepler Object of Interest (KOI) with which to test the efficacy of direct fits of ringed planets to *Kepler* data, we consider criteria for choosing candidates so as to maximize the productivity of the search. Since the optimal conditions for forming rings are still not well defined theoretically, we focus our attention on objects that we consider the most likely to yield meaningful constraints on potential ring systems by looking for planet candidates with the following characteristics: (1) long orbital periods, (2) large ice Roche Limits, (3) high signal-to-noise ratios (SNR), and (4) large apparent planetary radii.

We prefer long-period orbits for two reasons. First, dynamical effects such as stellar perturbations and Poynting–Robertson drag affect closer-in planets more strongly (Schlichting and Chang, 2011). Schlichting and Chang (2011) show that orbits with semimajor axes greater than 0.1 AU significantly increase expected ring lifetimes. Second, large semimajor axes allow for a higher diversity of possible ring compositions. While silicate-rich dense rings are theoretically possible (Schlichting and Chang, 2011), the only extensive ring system that we currently know of, Saturn's, is made of nearly pure water ice (Pilcher et al., 1970). And ice-rich materials could have mechanical properties that favor the formation and maintenance of dense rings Hedman (2015). Since long orbital periods ($\gtrsim 4.4$ yrs) are needed to be outside the ice line for our Sun, we target the planetary candidates with the longest orbital periods as most likely to harbor rings.

Those large orbital periods also have the benefit of yielding objects with larger Roche limits. True planetary rings that are unable to coagulate into discrete moons can only exist inside the planet's Roche limit, which we calculate for each candidate using the standard equation:

$$\mathscr{R} \approx 2.45 R_p \left(\frac{\rho_p}{\rho}\right)^{\frac{1}{3}} \tag{2}$$

where R_p is planet radius, ρ_p is the planets density, and ρ is the particle density (Carroll and Ostlie, 1996). Making use of Figure 7 of Fortney et al. (2007) to estimate the mass to each planet candidate, based on a probable radius, we can then determine the Roche limit for both ice ($\rho = 1\ \frac{\mathrm{g}}{\mathrm{cm}^3}$), and rock ($\rho = 3\ \frac{\mathrm{g}}{\mathrm{cm}^3}$). Larger Roche limits allow for more extensive ring systems with higher detectabilities.

All else being equal, a star with high signal-to-noise ratio (SNR) photometry will make for easier ring detection and/or tighter constraints on the presence of ring systems. Even large rings have relatively low detectabilities of order $10^{-4} - 10^{-3}$ (Barnes and Fortney, 2004). Because the presence of rings is easiest to observe in photometry during ingress and egress of the planet-ring system, a high SNR is particularly important because of the relatively short duration of ingress and egress.

Perhaps counterintuitively, a good exoring candidate will have a large initially inferred planet radius – so big that its planetary nature might be in question. Zuluaga et al. (2015) showed that a ringed planet will appear larger than the planet's actual radius due to the presence of rings. Thus abnormally large initial-guess planet radii can be an indication of rings – at least so long as they do not indicate that the candidate is really an M-dwarf. As an example of this radius excess

Table 1
Relevant parameters for our test case for a ring search, KOI-422.01. The planet mass is inferred from its radius following Fortney et al. (2007). Roche limits are given for the cases of icy ($\mathscr{R}_{\rm ice}$) or rocky ($\mathscr{R}_{\rm rock}$) ring particles. The true uncertainty associated with our calculated Roche Limits derives from the assumed planetary mass. We assume a stellar mass of 1.1 $M_\odot$ for KOI-422. The parameter b is the impact parameter, ϵ is eccentricity (representing a lower limit), c_1 and c_2 are the first two limb darkening coefficients (where $c_1 = u_1 + u_2$ and $c_2 = u_1 - u_2$ following Brown et al. (2001)), and χ^2 is the statistical distribution test. Coefficients for stars limb darkening are obtained from Sing (2010) Table 2, and Stellar temperatures are obtained from CFOP (the *Kepler* Community Follow-up Observing Program).

KOI	422.01
M_p (M_{Jup})	0.8 (assumed)
Period	809.014 ± 0.002 days (fit)
$\mathscr{R}_{ice}$ (R_{Jup})	2.45 (calculated)
$\mathscr{R}_{rock}$ (R_{Jup})	1.70 (calculated)
$\frac{\mathscr{R}_{ice}}{R_p}$	1.82 (calculated)
$\frac{\mathscr{R}_{rock}}{R_p}$	1.26 (calculated)
Temp. (K)	6242 ± 165 (Borucki et al., 2011)
R_s	1.34 ± 0.04$R_\odot$ (fit)
R_p	1.72 ± 0.06$R_{\rm Jup}$ (fit)
b	0.59 ± 0.04 (fit)
ϵ	0.69 ± 0.03 (fit)
c_1	0.34 ± 0.18(fit)
c_2	0.0 (fixed)
χ^2	1.19

effect, consider if an observer viewed Saturn from another star system. The observer would initially deduce the radius of Saturn to be as much as twice as large as the true radius due to the rings intercepting more stellar flux (Tusnski and Valio, 2011). Therefore, a search for ringed planets might strongly consider candidates with radii even larger than possible for non-irradiated gas planets (Fortney et al., 2007).

3.2. Observations

We obtain photometry for *Kepler* Objects of Interest from the publicly available MAST database. Using the criteria from Section3.1, we consider a set of four transiting planet candidates around which to search for rings: KOI-289.02, KOI-422.01, KOI-1353.01, and KOI-3541.01. An initial spherical fit to each of these lightcurve s shows no residuals indicative of possible ring systems. Therefore we focus just on KOI-422.01 to demonstrate the types of constraints that can and cannot be placed on potential ring systems based on transit photometry.

Table 1 shows the parameters of that test system, KOI-422.01. With an orbit period of 809.014 ± 0.002 days, *Kepler* only had a chance to see two transits. Even then, KOI-422.01 is still too close to its star to maintain icy rings.

The presearch data conditioned KOI-422 photometry displays few irregularities. We therefore adopt a minimalist approach to data reduction to avoid introducing artifacts. We tried three different approaches to remove out-of-transit variability: (1) applying a median boxcar filter with a period 6 times the transit duration (Barnes et al., 2015), (2) subtracting polynomial fits of the out-of-transit data around each transit, and (3) nothing. Although each approach differs in detail, the resulting lightcurve s show no significant trends relative to one another, and fits yield parameters that agree to within 1-sigma. We therefore elect to use the median boxcar filtered data for consistency with our own previous work (e.g., Ahlers et al., 2014; Barnes et al., 2015).

Table 2
Ring Fit Parameters. Ring Fit Parameters for lowest χ^2 vs τ values.

KOI-422.01				
Angle	90°	60°	45°	20°
R_s ($R_\odot$)	1.16 ± 0.08	1.18 ± 0.04	1.17 ± 0.04	1.12 ± 0.04
τ	1.	2.	5.	2
R_o (R_{Jup})	1.68 ± 0.13	1.66 ± 0.07.	1.77 ± 0.07	2.30 ± 0.12
b	1.82 ± 0.09	01.87 ± 0.04	1.86 ± 0.05	1.78 ± 0.05
ϵ	0.62 ± 0.04	0.63 ± 0.02	0.62 ± 0.02	0.65 ± 0.03
χ^2	1.38	1.31	1.30	1.26

4. Test case results

Because the spherical model shows no significant residuals that might indicate the presence of a ring system, we establish upper limits on rings surrounding one of our four candidates. We chose KOI-422.01 for this analysis for its large initial guess planet radius and long orbital period (the longest of our four candidates). Because cold gas giants with radii larger than $\sim 1.0 R_{\rm Jup}$ are neither seen nor predicted to exist (Fortney et al., 2007; Seager et al., 2007), we deduce that if KOI-422.01 is a planet, then it probably has rings. Also, with an orbital period of ~ 809 days, it is less likely that the host star's gravity and luminosity would adversely influence a ring system's stability.

We first consider the possibility of an asymmetric transit. As shown in Fig. 2, planets with significant obliquity (ϕ) and azimuth between $\psi = 0°$ and $\psi = 90°$ produce asymmetric transit lightcurve s in such a way as to be most easily detected. To test for such asymmetry we fit the KOI-422 lightcurve for a ringed planet with an obliquity of $\phi = 45°$ and azimuthal angle of $\psi = 45°$. We hold R_p constant at 1 $R_{\rm Jup}$ for KOI-422.01, assuming the highest possible planet radius as if this object were a ringed planet. The best-fit result using a spherical-planet model has $R_s = 1.1 \pm 0.03, R_o = 2.0 \pm 0.08, R_{ring} = 0.9 R_{\rm Jup}$ — and $\chi^2_r = 4.99$ (!). This remarkably high χ^2_r in relation to χ^2_{spher} indicates that any potential rings around KOI-422.01 cannot deviate far from an azimuthal angle with the north pole pointing towards or away from us.

Given the lack of evidence for transit asymmetry, then, we therefore hold ψ at 90° in subsequent fits to force the lightcurve to be symmetric. The obliquity angle ϕ is held constant on each fit, but we run separate fits with $\phi = 90°$, 60°, 45°, and 20° to explore parameter space. We keep the inner radius of the ring constant to 1.1 $R_{\rm Jup}$ to retain a gap between the ring and planet as would result from atmospheric drag. The normal optical depth τ is held constant to avoid degeneracies, but we again assign varying values of τ on successive fits to explore its effects (Fig. 4).

With these fixed values, we then fit the KOI-422 lightcurve for outer ring radius (R_o), star radius (R_s), eccentricity (ϵ), and impact parameter b using `transitfitter` for a sequence of fits, adjusting τ and ϕ on subsequent runs. Due to the weak dependence of eccentricity on the longitude of periapsis (Price et al., 2015), our fitted eccentricity fixes the transit to occur at periapsis, and therefore represents a lower limit on the actual planetary eccentricity. Our results are thus the most plausible orientation and size of a hypothetical ring system surrounding KOI-422.01. We also plot the resulting χ^2_r as a function of the input normal optical depth τ in Fig. 5.

Fits to the KOI-422.01 lightcurve using planets with low optical depth rings do a particularly poor job of replicating the data. These low-quality fits to translucent ring systems rule out optically thin rings with $\tau \sim 0.2$ (though not Jupiter-like rings with very low $\tau \sim 10^{-4}$). For all obliquities there is a minimum in the best-fit χ^2 around $1 \leq \tau \leq 2$. However even these χ^2 minima do not fit the data as well as the ringless, spherical-planet fit.

Therefore we interpret that if KOI-422.01 has rings, then they are below the threshold of detectability using our method. Possible reasons that we might not be able to identify a extant ring include: the fixed size of our assumed gap between the simulated ring and planet was too large, transit geometry if the planet has a low enough obliquity angle as to be near edge-on (i.e $\phi \sim 0°$), or if the rings could be smaller in radial extent than we assume based on Roche limit considerations.

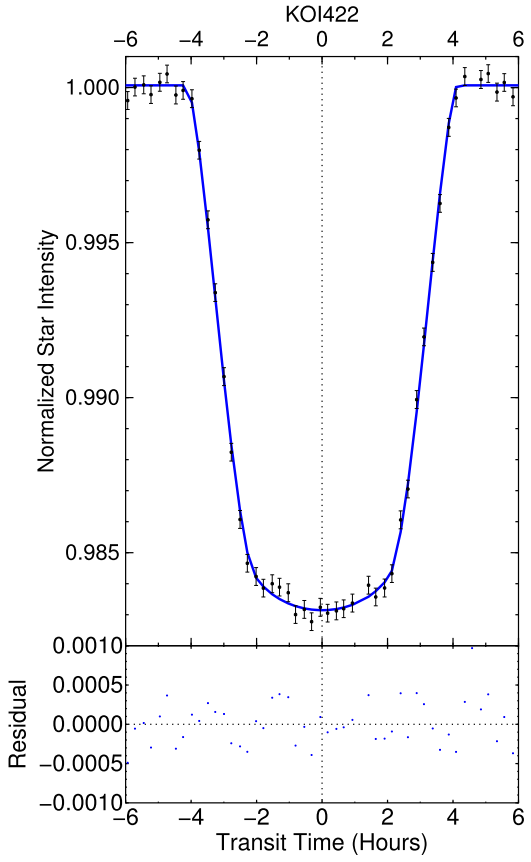

Fig. 4. KOI-422 spherical fit (top) and residual (bottom). The data represent unbinned, folded data for the two KOI-422.01 transit events. The errors represent the photometric error for each point.

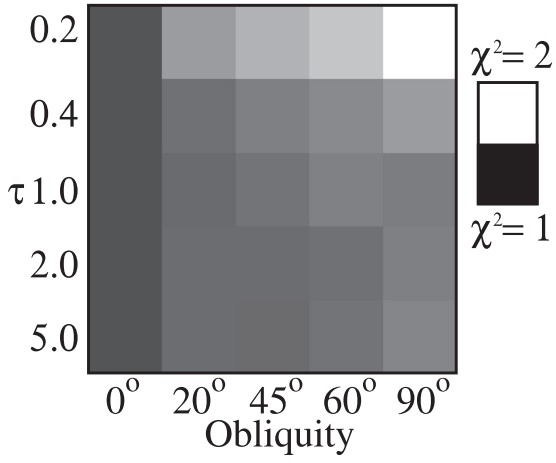

Fig. 5. Goodness-of-fit parameter χ^2 as a function of assigned normal ring optical depth τ under various scenarios fitting the transit lightcurveof KOI-422.01. Here we impose symmetric transits by fixing the azimuthal angle to $\psi = 90°$. The column at right corresponds to a planetary obliquity $\phi = 90°$, to its left is $\phi = 60°$, next is $\phi = 45°$, second from left shows $\phi = 20°$, and the left-hand column is a spherical (ringless) fit to the KOI-422.01 transit lightcurve. No ringed planet models the data as well as the ringless model.

5. Discussion and conclusion

In this pilot investigation we demonstrate a method for constraining the presence of ring systems around individual transiting exoplanets by analyzing their transit lightcurves. Specifically, we show that exoplanet candidate KOI-422.01 probably does not have large Saturn-type rings based on detailed transit lightcurve fitting using ringed-planet models.

Fits of specific lightcurve s using ringed planet models reveal myriad degeneracies. Both the planetary radius and cross-sectional area combined with opacity of the rings affect the total transit depth, for instance. After fixing the planet's radius, degeneracies remain between the rings' outer edge, the rings' optical depth, and the rings' opening angle.

However, the fits are very sensitive to *asymmetric* transits – ones where the projected rings show an azimuthal tilt relative to the planet's apparent path across the star. The intensity of the asymmetry is degenerate between this azimuthal angle and the rings' own asymmetry. However given the much easier case of detecting asymmetrically transiting ring systems, the best search for rings might be done in an ensemble, where the probability that EVERY system is viewed edge-on becomes very low.

Comprehensive fits to individual systems, particularly in the absence of any detected residual signal, requires significant processing power (at least the way that we do it). Given the aforementioned preference for asymmetric transits, a superior search strategy looking for unexplained residuals in a number of systems would be a rational first step. Such a search could have difficulty, however, in establishing quantitative upper limits on what ring systems could have been seen.

Despite our test target KOI-422 being one of the longest-period viable *Kepler* candidates, it still resides interior to the ice line of its host star. Given *Kepler*'s reaction-wheel shortened mission while targeting its prime field, the chances of detecting an exoring system around multiply-transiting planets may therefore be low. Single, non-repeating transits would improve the chances of observing a planet outside the ice line, but at the expense of certain knowledge of the planet's orbital period.

Therefore even a comprehensive survey of the *Kepler* data may not find ring systems because they may not exist in the parameter space in which we can look. A negative result might lend some support to the idea that ring formation and/or long-term stability may only be likely to occur under restricted conditions that include low temperatures (Hedman, 2015). But if the low-temperature rings hypothesis is correct, then we may need to wait for transits of very-long-period planets for our first detection.

Acknowledgments

The authors acknowledge funding support from an Idaho Space Grant Consortium Research Initiation Grant (NNX10AM75H). WTH thanks Dr. Christine Berven for serving on his thesis committee.

References

Ahlers, J.P., Seubert, S.A., Barnes, J.W., 2014. ApJ 786, 131.
Arnold, L., Schneider, J., 2004. A&A 420, 1153.
Barnes, J. W., Ahlers, J. P., Seubert, S. A., Relles, H. M., 2015. ApJ, in review.
Barnes, J.W., Fortney, J.J., 2003. ApJ 588, 545.
Barnes, J.W., Fortney, J.J., 2004. ApJ 616, 1193–1203.
Borucki, W.J., Koch, D.G., Basri, G., et al., 2011. ApJ 736, 19.
Braga-Ribas, F., Sicardy, B., Ortiz, J., et al., 2014. Nature.
Brown, T.M., Charbonneau, D., Gilliland, R.L., Noyes, R.W., Burrows, A., 2001. ApJ 552, 699.
Burns, J.A., Cuzzi, J.N., Durisen, R.H., Hamill, P., 1979. AJ 84, 1783–1801.
Burns, J.A., Simonelli, D.P., Showalter, M.R., et al., 2004. In: Bagenal, F., Dowling, T.E., McKinnon, W.B. (Eds.), Jupiter. The Planet, Satellites and Magnetosphere, pp. 241–262.
Canup, R.M., 2010. Nature 468, 943.
Carroll, B. W., Ostlie, D. A., 1996. An Introduction to Modern Astrophysics.
Charnoz, S., Dones, L., Esposito, L.W., Estrada, P.R., Hedman, M.M., 2009a. In: Dougherty, M.K., Esposito, L.W., Krimigis, S.M. (Eds.), Saturn from Cassini-Huygens, pp. 537.
Charnoz, S., Morbidelli, A., Dones, L., Salmon, J., 2009b. Icarus 199, 413.
Colwell, J.E., Nicholson, P.D., Tiscareno, M.S., et al., 2009. In: Dougherty, M.K., Esposito, L.W., Krimigis, S.M. (Eds.), Saturn from Cassini-Huygens, pp. 375.
Cruikshank, D.P., Matthews, M.S., 1995. Neptune and Triton. University of Arizona Press.
Cuzzi, J.N., Estrada, P.R., 1998. Icarus 132 (1), 1.
Dyudina, U.A., Sackett, P.D., Bayliss, D.D.R., et al., 2005. ApJ 618, 973.
Estrada, P.R., Durisen, R.H., Cuzzi, J.N., Morgan, D.A., 2015. Icarus 252, 415.

Fortney, J.J., Marley, M.S., Barnes, J.W., 2007. ApJ 659, 1661.
French, R., Nicholson, P., 2003. NASA Planetary Data System. USA_NASA_PDS_EBROCC_001.
French, R.G., Nicholson, P.D., Porco, C.C., Marouf, E.A., 1991. In: Bergstralh, J.T., Miner, E.D., Matthews, M.S. (Eds.), Uranus, pp. 327–409.
Galilei, G., 1989. Sidereus nuncius, or, The Sidereal messenger. Chicago: University of Chicago Press, 1989.
Hedman, M.M., 2015. ApJ 801, L33.
Horányi, M., Burns, J.A., Hedman, M.M., Jones, G.H., Kempf, S., 2009. In: Dougherty, M.K., Esposito, L.W., Krimigis, S.M. (Eds.), Saturn from Cassini-Huygens, pp. 511.
Hyodo, R., Charnoz, S., Ohtsuki, K., Genda, H., 2016. ArXiv e-prints 1609.02396.
Kenworthy, M. A., Mamajek, E. E., 2015. ArXiv e-prints 1501.05652.
Mamajek, E.E., Quillen, A.C., Pecaut, M.J., et al., 2012. AJ 143, 72.
Martins, J.H.C., Santos, N.C., Figueira, P., et al., 2015. A&A 576, A134.
Ohta, Y., Taruya, A., Suto, Y., 2009. Astrophys. J. 690, 1.
Ortiz, J.L., Duffard, R., Pinilla-Alonso, N., et al., 2015. A&A 576, A18.
Pilcher, C.B., Chapman, C.R., Lebofsky, L.A., Kieffer, H.H., 1970. Science 167, 1372.
Price, E.M., Rogers, L.A., Johnson, J.A., Dawson, R.I., 2015. ApJ 799, 17.
Ruprecht, J.D., Bosh, A.S., Person, M.J., et al., 2015. Icarus 252, 271.
Santos, N.C., Martins, J.H.C., Boué, G., et al., 2015. A&A 583, A50.
Schlichting, H.E., Chang, P., 2011. ApJ 734, 117.
Seager, S., Kuchner, M., Hier-Majumder, C.A., Militzer, B., 2007. ApJ 669, 1279.
Sing, D.K., 2010. A&A 510, A21.
Thiessenhusen, K.-U., Krivov, A., Krüger, H., Grün, E., 2002. Planet Space Sci. 50, 79.
Tusnski, L.R.M., Valio, A., 2011. Astrophys. J. 743, 97.
Tyler, G.L., Marouf, E.A., Wood, G.E., 1981. J. Geophys. Res. 86, 8699.
Zuluaga, J.I., Kipping, D.M., Sucerquia, M., Alvarado, J.A., 2015. ApJ 803, L14.